Intraband relaxation and temperature dependence of the fluorescence decay time of one-dimensional Frenkel excitons

Bednarz, M.; Malyshev, V. A.; Knoester, J.

Published in:
The Journal of Chemical Physics

DOI:
10.1063/1.1499483

Intraband relaxation and temperature dependence of the fluorescence decay time of one-dimensional Frenkel excitons: The Pauli master equation approach

M. Bednarz
Institute for Theoretical Physics and Material Science Center, University of Groningen, Nijenborgh 4, 9747 AG Groningen, The Netherlands and Institute of Theoretical Physics, Warsaw University, Hoża Street 69, 00-681 Warsaw, Poland

V. A. Malyshev
National Research Center "Vavilov State Optical Institute," Birzhevaya Liniya 12, 199034 Saint-Petersburg, Russia

J. Knoester
Institute for Theoretical Physics and Material Science Center, University of Groningen, Nijenborgh 4, 9747 AG Groningen, The Netherlands and Department of Chemistry, Massachusetts Institute of Technology, Cambridge, Massachusetts 02139

(Received 21 March 2002; accepted 17 June 2002)

In molecular J-aggregates one often observes an increase of the fluorescence decay time when increasing the temperature from 0 K. This phenomenon is usually attributed to the thermal population of the dark Frenkel exciton states that lie above the superradiant bottom state of the exciton band. In this paper, we study this effect for a homogeneous one-dimensional aggregate in a host medium and we model the scattering between different exciton states as arising from their coupling to the host vibrations. A Pauli master equation is used to describe the redistribution of excitons over the band. The rates entering this equation are calculated within the framework of first-order perturbation theory, assuming a linear on-site interaction between excitons and acoustic phonons. Solving the master equation numerically for aggregates of up to 100 molecules, we calculate the temperature dependence of the fluorescence kinetics in general and the decay time scale in particular. The proper definition of the fluorescence decay time is discussed in detail. We demonstrate that, even at a quantum yield of unity, the possibility to directly interpret fluorescence experiments in terms of a simple radiative time scale depends crucially on the initial excitation conditions in combination with the competition between spontaneous emission and intraband phonon-assisted relaxation. © *2002 American Institute of Physics.* [DOI: 10.1063/1.1499483]

I. INTRODUCTION

The concept of one-dimensional (1D) Frenkel excitons[1,2] has proven to be very useful in explaining the low-temperature optical properties of molecular aggregates and conjugated polymers (for reviews, see Refs. 3–5, and references therein). One of the remarkable features of 1D Frenkel exciton systems is that only a few states accumulate the entire oscillator strength. As long as the chain length is small compared to the emission wavelength, this leads to an enhancement of the corresponding spontaneous emission rates by approximately a factor of N over the radiative rate of a single molecule. Here N denotes the number of molecules in the chain or, in the case of a disordered chain, the number of molecules within a localization domain of the excitons.[6–8] For a perfectly ordered aggregate whose length exceeds the emission wavelength, the enhancement factor saturates at the number of molecules within this wavelength.[9,10]

Experiments on various types of cyanine J-aggregates in (glassy) solution, in particular 1,1'-diethyl-2,2'-cyanine (PIC),[11–15] 5,5',6,6'-tetrachloro-1,1'-diethyl-3,3'-di(4-sulfobutyl)-benzimidazolo carbocyanine (TDBC),[16] 1,1'-diethyl-3,3'-bis(sulfopropyl)-5,5',6,6'-tetrachlorobenzimidacarbocyanine (BIC),[17] and 3,3'-bis(sulfopropyl)-5,5'-dichloro-9-ethylthiacarbocyanine (THIATS),[18] have revealed that the exciton radiative lifetime grows with increasing temperature. Typically, the temperature dependence consists of a plateau that extends to several tens of Kelvin, followed by a powerlike growth of the lifetime at higher temperatures. This slowing down of the aggregate's radiative dynamics is usually attributed to the thermal population of higher exciton states, which in J-aggregates have oscillator strengths that are small compared to those of the optically active states near the bottom of the exciton band.[8,12,13]

The first attempt to fit the experimental data on PIC reported in Ref. 11 was based on a microscopic model of Frenkel excitons coupled to the vibrations of the aggregate itself.[19] An integrodifferential equation of motion for the populations of the exciton states, derived by eliminating the phonon variables through a factorization, was used to describe the exciton dynamics. Assuming this dynamics to be dominated by an optical phonon of suitable frequency, the experimental data were fitted reasonably well over the entire temperature range. However, after correction of the experimental data for the temperature dependence of the quantum

yield,[15] it turned out impossible to fit the experiments by the theory developed in Ref. 19, unless PIC J-aggregates were assumed to be two-dimensional.[20] The issue of structure and dimensionality of cyanine J-aggregates in solution is a difficult and intriguing one. While usually assumed to be 1D, the nearly linear temperature dependence of the exciton radiative lifetime measured in BIC aggregates has led to the conclusion that these aggregates would be really two-dimensional as well.[17] The rationale for this conclusion was the similarity of this (linear) dependence to the behavior observed in quasi-two-dimensional semiconductor nanostructures.[21] On the other hand, the exciton radiative lifetime of THIATS aggregates can be understood in terms of a one-dimensional model, provided that the Davydov splitting[2] is correctly accounted for.[18] Moreover, recent cryogenic transmission electron microscopy images have revealed that PIC aggregates in solution do in fact assume a one-dimensional structure, in which a few molecular chains bundle up to form one aggregate.[22]

The state of affairs described above calls for a renewed critical discussion of the temperature dependent radiative lifetime of J-aggregates. The present paper contributes several new elements to this discussion. In particular, we will point out the important role of the experimental excitation conditions in relation to the competition between spontaneous emission and vibration-assisted intraband exciton relaxation.

It is important to realize that in all the above quoted measurements of the exciton radiative lifetime,[11–18] the system was excited in the blue tail of the absorption band, while the fluorescence was observed either within the entire band or at a particular energy close to the absorption maximum. Thus, between the absorption and emission events an additional step existed: the vibration-assisted relaxation from the initially excited states to the radiating ones. From this it is immediately clear that the ratio between the rates of two processes, namely vibration-assisted intraband exciton relaxation and exciton spontaneous emission, determines the kinetics of the fluorescence decay. Two limiting cases can be distinguished. If the intraband relaxation is faster than the spontaneous emission, the population of the excited state is rapidly transferred to the radiating state, whereupon this state will slowly (on the scale of the intraband relaxation) radiate. In this limit, it is the *spontaneous emission* rate that determines the rate of the exciton fluorescence decay. Analyzing this decay properly (quantum yield correction, etc.), one may extract from such measurements the actual exciton radiative decay time. In the opposite limit, it is the slow *intraband relaxation* that acts as bottleneck in the exciton fluorescence decay and thus governs the measured lifetime. It is then unlikely that one obtains accurate information about the exciton radiative lifetime from such experiments. Rather, it seems that then the only way to properly measure the exciton radiative lifetime is to resonantly excite the exciton fluorescence. This may be done using accumulated photon echo experiments. However, as we will show in this paper, even under resonant excitation, it is not always easy to extract information about the exciton radiative lifetime from spectroscopic data.

The goal of this paper, motivated by the above observations, is a systematic analysis of the temperature dependence of the fluorescence decay time of 1D Frenkel excitons under various excitation conditions, taking into account the effects of intraband exciton relaxation. As the physics of the above noted effects does not depend strongly on whether the system is disordered or not,[23] we will restrict our study to the simplest case of an ordered aggregate, where these effects can be demonstrated in their purest form. A study of the additional effects of disorder will be deferred to a later publication. We will assume that the relaxation dynamics of the excitons in the aggregate is governed by their coupling to vibrations in the host medium,[24–27] rather than to vibrations of the aggregate itself.[19] The exciton dynamics will be described at the level of a Pauli master equation for the populations of the exciton states. The vibration-assisted population transfer rates governing this equation are obtained within a first-order perturbation expansion in a linear exciton–phonon interaction. As we mainly aim to study the low-temperature behavior of the exciton fluorescence, we focus on a coupling to acoustic phonons. The thus obtained master equation is solved numerically to describe the fluorescence kinetics both as a function of time and temperature. As the case of fast relaxation is rather uninteresting (because the excitons reach thermal equilibrium before emission), we will throughout this paper mostly focus on the case of slow relaxation. By this we mean that at least the zero-temperature intraband relaxation rates are small compared to the superradiant emission rate.

This paper is organized as follows: In Sec. II, we present the model Hamiltonian of Frenkel excitons interacting with host vibrations. The Pauli master equation for the exciton populations is introduced in Sec. III. Section IV deals with calculating the exciton scattering rates that enter this equation. In Sec. V, we demonstrate that the proper definition of a fluorescence decay time is a subtle problem and is in fact affected by the competition between radiative decay and intraband relaxation. Our numerical results for the temperature dependence of the exciton fluorescence decay time in different limits of this competition and for different initial excitation conditions are given and discussed in Sec. VI. Finally, we conclude in Sec. VII.

II. MODEL HAMILTONIAN

We model an aggregate as N ($N \gg 1$) optically active two-level molecules forming a regular 1D lattice with spacing a. If the aggregate is considered fixed in its equilibrium geometry, its optical excitations are described by the Frenkel exciton Hamiltonian,[2]

$$H_{\mathrm{ex}} = \sum_{n=1}^{N} \epsilon_n^0 |n\rangle\langle n| + \sum_{n,m}^{N} J_{nm} |n\rangle\langle m|. \tag{1}$$

Here, $|n\rangle$ is the state with molecule n of the aggregate excited and all other molecules in their ground state. This basis state has energy $\epsilon_n^0 = \epsilon_0 + U_n^0$, with ϵ_0 the energy of the excited state of an isolated molecule and $U_n^0 = \Sigma_s U_{ns}^0$ the shift due to the interactions U_{ns} of the nth excited molecule with all other aggregate and host molecules in their ground states

(the superscript "0" indicates that these interactions are taken for the molecular equilibrium positions). As we will not consider effects of electronic disorder, all energies ϵ_n are assumed identical and from now on will be set to zero. Likewise, disorder in the excitation hopping integrals J_{nm} will not be considered. These interactions are assumed to be of dipole–dipole origin, $J_{nm}=-J/|n-m|^3 (J_{nn}\equiv 0)$, where $-J$ is the nearest-neighbor coupling. We will take J to be positive, as is appropriate for J-aggregates.[11–13] Then, the optically allowed states are those in the vicinity of the bottom of the exciton band.

Accounting for all dipole–dipole interactions, the Hamiltonian Eq. (1) can be diagonalized with a precision of the order of N^{-1} (see Ref. 28),

$$H_{\mathrm{ex}}=\sum_K E_k |k\rangle\langle k|, \tag{2}$$

with the new basis

$$|k\rangle=\left(\frac{2}{N+1}\right)^{1/2}\sum_{n=1}^{N} \sin\left(\frac{\pi k n}{N+1}\right)|n\rangle, \tag{3a}$$

and

$$E_k=-2J\sum_{n=1}^{N}\frac{1}{n^3}\cos\left(\frac{\pi k n}{N+1}\right). \tag{3b}$$

Here, $k=1,2,\ldots,N$. For future use it is convenient to introduce the compact notation (wavenumber) $K=\pi k/(N+1)$. The state $k=1$ lies at the bottom of the exciton band. Near the bottom ($k\ll N$ or $K\ll 1$) and in the limit of large N,[28] the exciton dispersion relation reads

$$E_k=-2.404J+J\left(\tfrac{3}{2}-\ln K\right)K^2. \tag{4}$$

For comparison, within the nearest-neighbor approximation one obtains $E_k=-2J+JK^2$.

The oscillator strengths of the exciton states near the bottom of the band are given by

$$F_k=\frac{2}{N+1}\left(\sum_{n=1}^{N}\sin Kn\right)^2=\frac{1-(-1)^k}{N+1}\frac{4}{K^2}. \tag{5}$$

Here, the oscillator strength of a single molecule is set to unity. According to Eq. (5), the bottom state $k=1$ (with energy $E_1=-2.404J$) accumulates almost the entire oscillator strength, $F_1=0.81(N+1)$; it is referred to as the superradiant state. The oscillator strengths of the other odd states ($k=3,5,\ldots$) are much smaller, $F_k=F_1/k^2$, while the even states ($k=2,4,\ldots$) carry no oscillator strength at all, $F_k=0$. We note that the small corrections to the sine wave functions in Eq. (3a) due to the long-range dipole–dipole interactions, lead to a small change in the superradiant prefactor, which for aggregates of 100 molecules reads $0.84(N+1)$ instead of $0.81(\mathrm{N}+1)$.[7]

Thermal motion of the surrounding molecules as well as the molecules of the aggregate itself, result in fluctuations of both the on-site energies ϵ_n (due to the fluctuations in $U_n=\Sigma_s U_{ns}$) and the dipole–dipole interactions J_{mn}. This causes scattering of the excitons from one state $|k\rangle$ to other states $|k'\rangle$. In this paper, we only deal explicitly with the on-site part of the exciton-vibration coupling and neglect the intermolecular part. Assuming linear coupling, the relevant interaction Hamiltonian reads[2]

$$H_{\mathrm{ex-vib}}=\sum_{n=1}^{N}\sum_q V_{nq}|n\rangle\langle n|a_q+\mathrm{h.c.}, \tag{6}$$

Here, V_{nq} is the on-site coupling constant of the normal vibration mode q to the molecule n and the q-summation runs over all normal modes of the entire system (aggregate +host). Furthermore, a_q and $a_q^\dagger$ are the usual creation and annihilation operators. As our main interest lies in the low-temperature (<100 K) behavior of the exciton radiative lifetime, we will focus on the interaction of excitons with acoustic phonons of relatively long wavelengths. We then have (see Ref. 2 and Appendix A)

$$V_{nq}=i\left(\frac{|\mathbf{q}|}{2Mv_\alpha}\right)^{1/2}\chi_{nq}\,e^{i\mathbf{q}\cdot\mathbf{R}_n}, \tag{7}$$

where the mode label now stands for $q=(\mathbf{q},\alpha)$, $\mathbf{q}$ being the wave vector of the acoustic mode q and α labeling two transverse ($\alpha=1,2$) and one longitudinal ($\alpha=3$) polarizations. Furthermore, M denotes the mass of the entire system, v_α is the velocity of sound waves with polarization α, and $\mathbf{R}_n$ is the position vector of the nth molecule in the aggregate. Finally, χ_{nq} [defined in Eq. (A7)] does not depend on the magnitude of $\mathbf{q}$, while its dependence on the orientation of $\mathbf{q}$ is smooth. The $\sim\sqrt{|\mathbf{q}|}$ scaling of V_{nq} expresses the fact that the coupling of excitons to acoustic phonons diminishes in the long wavelength limit.

Within the exciton representation, the Hamiltonian Eq. (6) takes the form

$$H_{\mathrm{ex-vib}}=\sum_{k,k'=1}^{N}\sum_q V_{kk'}^q|k\rangle\langle k'|a_q+\mathrm{h.c.}, \tag{8}$$

where the exciton–phonon coupling $V_{kk'}^q$ is given by

$$V_{kk'}^q=i\left(\frac{|\mathbf{q}|}{2Mv_\alpha}\right)^{1/2}\times\frac{2}{N+1}\sum_{n=1}^{N}\chi_{nq}e^{i\mathbf{q}\cdot\mathbf{R}_n}\sin(Kn)\sin(K'n). \tag{9}$$

In this paper, we distinguish two models for the $\mathbf{R_n}$-dependence of χ_{nq}. In the first one, we assume no dependence, $\chi_{nq}=\chi_q$. This corresponds to the situation of an aggregate placed in a crystalline host. In the second model, χ_{nq} is regarded a stochastic function of the molecular position, having the correlation properties,

$$\langle\chi_{nq}\rangle=0, \tag{10a}$$

$$\langle\chi_{nq}\chi_{n'q}\rangle=\chi_q^2\delta_{nn'}. \tag{10b}$$

This may serve as a model to describe exciton–phonon coupling for an aggregate placed inside a disordered host. The Kronecker symbol in Eq. (10b) implies that the surroundings of different molecules in the aggregate are not correlated.

Throughout this paper, we assume that the exciton–phonon coupling is too weak to renormalize the exciton band structure and wave functions (no polaron effects) and, thus,

can be treated as a perturbation. This allows us, first, to calculate the rates of the intraband exciton scattering ($k \to k'$) using first-order perturbation theory, and second, to exploit the Pauli master equation for describing the kinetics of the intraband exciton relaxation. As we will see, both models for χ_{nq} introduced above, lead to analytical expressions for the exciton scattering rates.

III. THE PAULI MASTER EQUATION

In order to describe the kinetics of intraband exciton relaxation, we employ the Pauli master equation for the populations $P_k(t)$ of the exciton states,

$$\dot{P}_k = -\gamma_k P_k + \sum_{k'} (W_{kk'} P_{k'} - W_{k'k} P_k). \tag{11}$$

Here, the dot denotes the time derivative, $\gamma_k = \gamma_0 F_k$ is the spontaneous emission rate of the kth exciton state, which is enhanced relative to the single-molecule emission rate γ_0 by a factor of F_k given by Eq. (5), and $W_{kk'}$ is the rate of phonon-assisted scattering of excitons from state k' to state k. Within first-order perturbation theory, the latter reads

$$W_{kk'} = 2\pi \sum_q |V^q_{kk'}|^2 [n_q \delta(E_k - E_{k'} - \omega_q) + (1+n_q)\delta(E_k - E_{k'} + \omega_q)], \tag{12}$$

where $V^q_{kk'}$ is given by Eq. (9) and $n_q = [\exp(\omega_q/T) - 1]^{-1}$ is the thermal occupation of the qth acoustic mode, which has energy ω_q ($\hbar = k_B = 1$). In the next section, we will use Eq. (12) to determine the scattering rates for crystalline and glassy hosts. At this moment, we restrict ourselves to the general observation that Eq. (12) implies these rates to obey the principle of detailed balance,

$$W_{kk'} = W_{k'k} \exp\left(\frac{E_{k'} - E_k}{T}\right), \tag{13}$$

which guarantees that eventually the excitons will arrive at the proper equilibrium state, characterized by the Boltzmann distribution over energy.

The initial conditions to Eq. (11) depend on the excitation conditions. In the experiments on J-aggregates reported in Refs. 11–18, the fluorescence was observed after exciting weakly allowed excitons in the high-energy tail of the J-bands. In our numerical calculations, we will consider in addition to such blue-tail excitation, also the case of resonant excitation, where only the superradiant bottom state ($k=1$) is initially excited. The numerical procedure for solving Eq. (11) with the proper initial conditions is described in Appendix B.

The presence of two types of rates in the Master equation (11), namely, for spontaneous emission and intraband relaxation, makes the competition between both types of processes explicit. Throughout this paper, we will define the limit of slow relaxation through the relation $W_{12}(T=0) \ll \gamma_1$, which implies that at zero temperature, the phonon-induced transfer between the two bottom states of the exciton band is small compared to the superradiant emission rate of the bottom state.

IV. INTRABAND EXCITON SCATTERING RATES

We now turn to evaluating the scattering rates $W_{kk'}$ given by Eq. (12). To this end, we first replace the summation over the acoustic modes by an integration according to the standard rule,

$$\sum_q = \sum_{\alpha=1}^{3} \sum_{\mathbf{q}} \to \frac{\mathcal{V}}{(2\pi)^3} \sum_{\alpha=1}^{3} \int d\mathbf{q}, \tag{14}$$

where $\mathcal{V}$ is the quantization volume. Next, to simplify the algebra, we will restrict ourselves to an isotropic model for the acoustic phonons, implying equal speed for transverse and longitudinal sound waves, $v_1 = v_2 = v_3 = v$. Then $\omega_q = v|\mathbf{q}|$, so that Eq. (14) becomes

$$\sum_q = \sum_{\mathbf{q}} \sum_{\alpha=1}^{3} \to \frac{\mathcal{V}}{(2\pi v)^3} \sum_{\alpha=1}^{3} \int d\Omega_{\mathbf{q}} \int d\omega_q \, \omega_q^2, \tag{15}$$

where the first integration is over the orientations of $\mathbf{q}$. Due to the δ-functions in Eq. (12), the integration over ω_q can be performed explicitly. This leads to the substitution $|\mathbf{q}| = |E_k - E_{k'}|/v$ in any function that depends on $|\mathbf{q}|$.

A. Glassy host

For an aggregate embedded in a glassy host, χ_{nq} is a stochastic function with correlation properties given by Eq. (10). This allows us to find an analytical expression for the average of $W_{kk'}$. Namely, using the equality

$$\left\langle \left| \sum_{n=1}^{N} \chi_{nq} e^{i\mathbf{q}\cdot\mathbf{R}_n} \sin(Kn)\sin(K'n) \right|^2 \right\rangle = |\chi_q|^2 \sum_{n=1}^{N} \sin^2(Kn)\sin^2(K'n) = \frac{1}{4}|\chi_q|^2 (N+1)$$

in Eq. (12) and performing the integrations over ω_q and $\Omega_{\mathbf{q}}$, we obtain

$$W_{kk'} = \frac{W_0^{\mathrm{gl}}}{N+1} \left| \frac{E_k - E_{k'}}{J} \right|^3 \{\Theta(E_k - E_{k'}) n(E_k - E_{k'}) + \Theta(E_{k'} - E_k)[1 + n(E_{k'} - E_k)]\}, \tag{16}$$

with

$$W_0^{\mathrm{gl}} = \frac{J^3 \mathcal{V}}{8\pi^2 v^5 M} \sum_{\alpha=1}^{3} \int d\Omega_{\mathbf{q}} |\chi_q|^2. \tag{17}$$

Here, $\Theta(x) = 1$ for $x > 0$ and $\Theta(x) = 0$ otherwise. As is seen, in the glassy-host model $W_{kk'}$ scales inversely proportional to $N+1$, which is similar to the scaling obtained within the stochastic fluctuation model of exciton–phonon coupling (see, e.g., Ref. 29). The cubic dependence of $W_{kk'}$ in Eq. (17) on $|E_k - E_{k'}|$, however, sharply contrasts with the Lorentzian dependence obtained within the stochastic fluctuation model, and causes the hopping process to slow down with decreasing energy mismatch, i.e., towards the bottom of the exciton band.

B. Crystalline host

For an aggregate embedded in a crystalline host, we have $\chi_{nq}=\chi_q$, which can be taken out of the summation in Eq. (9). The remaining geometrical series yields

$$V^q_{kk'}=\frac{1}{N+1}\left(\frac{|\mathbf{q}|}{2Mv}\right)^{1/2}\chi_q \times\sin Q\,[1-(-1)^{k+k'}e^{iQ(N+1)}] \times\frac{\sin K\sin K'}{[\cos K'-\cos(K+Q)][\cos K'-\cos(K-Q)]}, \tag{18}$$

where $Q=|\mathbf{q}|a\cos\theta$, θ being the angle between the phonon wave vector $\mathbf{q}$ and the aggregate axis.

Let us now estimate the value of Q, which can be done using $|\mathbf{q}|=|E_k-E_{k'}|/v$ (see above). Then, for the exciton states near the bottom of the band (the region of primary interest), where $K,K'\ll 1$, we have $Q\sim(aJ/v)|(3/2-\ln K)K^2-(3/2-\ln K')K'^2|$. Typical parameter values are $a=10^{-7}$ cm, $J=600$ cm^{-1} $(2\times10^{13}\,\mathrm{s}^{-1})$, and $v=5\times10^5$ cm/s. Thus, the factor $aJ/v\approx 4$, i.e., of the order of unity. This fact and the quadratic scaling of Q with both K and K' allows us to neglect Q as compared to K and K' in the denominator of Eq. (18) as well as to substitute $\sin Q$ by Q. We also recall that χ_q is a smooth function of θ (see Appendix A), and thus can be replaced by a constant when integrating over the orientations of $\mathbf{q}$ in Eq. (12). With these simplifications, the latter integration can be performed analytically, leading to

$$W_{kk'}=\frac{W_0^{\mathrm{cr}}}{(N+1)^2}\sin^2K\sin^2K'\frac{|E_k-E_{k'}|^5}{J^5(\cos K-\cos K')^4} \times f[X(|E_k-E_{k'}|)] \times\{\Theta(E_k-E_{k'})n(E_k-E_{k'})+\Theta(E_{k'}-E_k) \times[1+n(E_{k'}-E_k)]\}, \tag{19}$$

where we introduced

$$W_0^{\mathrm{cr}}=\frac{a^2J^5\mathcal{V}}{3\pi v^7M}\sum_{\alpha=1}^{3}|\chi_q|^2, \tag{20a}$$

$$X(|E_k-E_{k'}|)=\frac{|E_k-E_{k'}|a}{v}(N+1), \tag{20b}$$

$$f(X)=1-(-1)^{k+k'}\frac{3}{X}\left[\left(1-\frac{2}{X^2}\right)\sin X+\frac{2}{X}\cos X\right]. \tag{20c}$$

We first note that the sine-functions in Eq. (19) reflect a strong suppression of scattering for the exciton states near the bottom of the band as compared to those in the center of the band. Second, the scattering between energetically close exciton states is less probable than between well separated ones (independent of their location within the band), because the factor $|E_k-E_{k'}|^5/(\cos K-\cos K')^4$ is roughly proportional to $|E_k-E_{k'}|$. Finally, it turns out that in practice the energy dependent factor $f(X)$ is always of the order of unity and does not yield a further suppression of the scattering rate. To see this, we first estimate X, which is obviously smallest for the two bottom states, $k=1$ and $k'=2$. Using Eq. (4), one thus obtains a minimal value of X given by $X_{\min}\approx(9\pi^2/2N)(aJ/v)$. We have estimated before that $aJ/v\approx 4$; moreover, in practice aggregate (coherence) lengths are limited to a few hundred molecules or less. We thus find that $X_{\min}\geqslant 1$, which from Eq. (20c) is seen to give values for f that are indeed of the order of unity.

V. DEFINING THE FLUORESCENCE DECAY TIME

To characterize the fluorescence decay that follows a short-pulse excitation at $t=0$, it is most convenient to have a single decay time. The definition of such a time is straightforward only for monoexponential decay, which, as we will see in Sec. VI does generally not take place. In addition, we will see that, even if a decay time seems straightforward to define, it may not always relate to a time scale of radiative emission. In this section, we address the two most obvious definitions of a fluorescence decay time and, by applying these definitions to the analytically solvable example of an exciton ''band'' consisting of two states only, we explain the nature of the problems that may arise and how they are affected by the experimental conditions.

The quantity observed in a fluorescence experiment is the radiative intensity $I(t)$, which is the number of emitted photons per unit time. Obviously, this equals the rate of loss of total exciton population, $I(t)=-\dot{P}(t)$, with $P(t)=\Sigma_k P_k(t)$. As in multilevel systems $I(t)$ generally does not show a monoexponential decay, it is mostly impossible to obtain a lifetime from a simple exponential fit. The simplest solution is to define a decay time, τ_e, as the time it takes the intensity to decay to $1/e$ of its peak value $I(t_{\mathrm{peak}})$,

$$I(t_{\mathrm{peak}}+\tau_e)=I(t_{\mathrm{peak}})/e. \tag{21}$$

We note that for blue-tail excitation generally $t_{\mathrm{peak}}\neq 0$. Alternatively, and maybe mathematically somewhat better-founded, one may define a lifetime, τ, as the expectation value of the photon emission time, given by

$$\tau=\int_0^\infty dt\,I(t)\,t=\int_0^\infty dt\,P(t). \tag{22}$$

Clearly, for monoexponential decay, $P(t)=\exp(-t/\tau)$, Eq. (22) gives the appropriate decay time τ. However, also for nonexponential fluorescence kinetics, the thus defined decay time seems to make sense. This indeed turns out to be correct, unless the total population kinetics consists of a large-weight component that rapidly decays and a much smaller-weight very slow component, comparable in integrated area to the fast component. Then, the tail contribution may mask the decay time of the fast component, which for all practical purposes should be considered the proper decay time. It appears that such a peculiar situation may easily occur in the case of J-aggregate fluorescence, in particular in the limit where the intraband relaxation is slow compared to the spontaneous emission from the superradiant bottom state.

To demonstrate this, we consider a model of two exciton levels, labeled $k=1$ and $k=2$. Level 1 is lowest in energy

and has a radiative emission rate γ_1, while level 2 is dark. We will assume that level 1 is initially excited. The Pauli master equation (11) now reduces to

$$\dot{P}_1 = -(\gamma_1 + W_{21})P_1 + W_{12}P_2, \tag{23a}$$

$$\dot{P}_2 = -W_{12}P_2 + W_{21}P_1, \tag{23b}$$

with initial conditions $P_1(0)=1$, $P_2(0)=0$. Solving Eq. (23) through Laplace transformation, yields for the total population, $P(t)=P_1(t)+P_2(t)$, the result

$$P(t) = \frac{\gamma_1}{\lambda_1 - \lambda_2}\left[\left(1 + \frac{W_{12}}{\lambda_2}\right)e^{\lambda_2 t} - \left(1 + \frac{W_{12}}{\lambda_1}\right)e^{\lambda_1 t}\right], \tag{24}$$

where

$$\lambda_{1,2} = -\tfrac{1}{2}(\gamma_1 + W_{12} + W_{21}) \pm \tfrac{1}{2}\sqrt{(\gamma_1 + W_{12} + W_{21})^2 - 4\gamma_1 W_{12}}. \tag{25}$$

Substituting Eq. (24) into Eq. (22), we arrive at the exact result

$$\tau = \frac{1}{\gamma_1}\left(1 + \frac{W_{21}}{W_{12}}\right). \tag{26}$$

From this it follows that at high temperatures ($T \gg E_2 - E_1$ and thus $W_{21} = W_{12} \equiv W$), one will get $\tau = 2\gamma_1^{-1}$, independently of the relation between W and γ_1. In the fast-relaxation limit [defined as $W_{12}(T=0) \gg \gamma_1$, implying $W \gg \gamma_1$ as well], this result is not surprising, because the population is then distributed uniformly over the two levels before the emission occurs. As only the lower level is radiating, this naturally leads to the effective division of the decay rate of level 1 by a factor of 2. However, in the limit of slow relaxation at the temperature considered [i.e., not only $W_{12}(T=0) \ll \gamma_1$, but also $W \ll \gamma_1$], the above result seems physically counterintuitive, because in this limit only a small part of the population can be transferred to the upper (dark) level before the lower level radiates, so that the upper level remains almost unpopulated. One thus expects to find a fluorescence decay time $\tau = \gamma_1^{-1}$, which obviously contradicts the exact result.

In order to discover the nature of the above contradiction, let us analyze in more detail the high-temperature kinetics of the total population in the slow-relaxation limit ($W \ll \gamma_1$),

$$P(t) = \left(1 - \frac{W}{\gamma_1}\right)e^{-\gamma_1 t} + \frac{W}{\gamma_1}e^{-Wt}. \tag{27}$$

This kinetics contains a fast exponential (first term) and a much slower one (second term). The fast component has the dominant weight, $1 - W/\gamma_1 \approx 1 \gg W/\gamma_1$; this reflects the fact that state 1 carries nearly all population, which decays rapidly with the decay time γ_1^{-1}. The much slower second term of the kinetics describes the decay of that (small) part of the total population that is transferred to level 2. Substituting Eq. (27) into Eq. (22) yields $\tau = 2\gamma_1^{-1}$, i.e., twice as large as expected from the physical arguments. This originates from the long-time tail in the second term, which gives, despite its small weight, a contribution to τ that is exactly equal to the one from the fast component.

In the opposite limit of fast relaxation, $W \gg \gamma_1$, we have

$$P(t) = \frac{\gamma_1}{4W}e^{-2Wt} + \left(1 - \frac{\gamma_1}{4W}\right)e^{-(\gamma_1/2)t}. \tag{28}$$

The first term, having a small weight, describes the fast (on the scale of $1/\gamma_1$) equilibration of the population over both levels. After that, the total population decays with the rate $\gamma_1/2$. We now arrive at $\tau = 2\gamma_1^{-1}$, which meets our physical expectation. Thus, in the fast-relaxation limit the definition Eq. (22) as fluorescence decay time seems to work properly.

To end this section, we reconsider the slow- and fast-relaxation limits, but now using τ_e for the decay time. In the slow-relaxation limit, $W \ll \gamma_1$, the intensity analog of Eq. (27) reads

$$I(t) = \gamma_1 e^{-\gamma_1 t} + \frac{W^2}{\gamma_1}e^{-Wt}. \tag{29}$$

Obviously, the second (slower) exponential has a negligible weight compared to the first (fast) one and we arrive at $\tau_e = \gamma_1^{-1}$, which is the physically expected value and does not suffer from the long-time tail.

In the fast-relaxation limit the intensity analog to Eq. (28) is given by

$$I(t) = \frac{\gamma_1}{2}\left(e^{-2Wt} + e^{-\frac{\gamma_1}{2}t}\right). \tag{30}$$

Here, the fast and slow components have equal weights, so that the intensity will decay rapidly (within $t \approx W^{-1}$) to half of its initial value, $I(0)=\gamma_1$. This reflects the already encountered fact that due to the fast transfer of population to level 2, the effective radiative constant is reduced from γ_1 to $\gamma_1/2$. It is straightforward to generalize this to the situation where l nonradiating levels are rapidly populated due to intraband relaxation from the superradiant level. At time zero, only the lowest state is populated, and the intensity is given by its decay rate γ_1. However, the population of that state is very rapidly (within a time $\sim 1/W \ll 1/\gamma_1$) redistributed over all l states, which will cause the effective rate to drop by a factor $l+1$ and thus also give an intensity drop from γ_1 to $\gamma_1/(l+1)$ over a time scale $1/W$. This results in a value for τ_e in the order of the inverse relaxation rate $(1/W)$, which has nothing to do with the actual radiative emission time scale in the system.

In conclusion, both most obvious definitions of the fluorescence decay time, τ and τ_e, may lead to counterintuitive results when trying to interpret them as exciton radiative lifetimes. This is unavoidable, due to the role of intraband relaxation, and simply means that all such measures should be considered with care and in relation to the experimental conditions. In the next section, we will see the above peculiarities show up for actual aggregates as well.

VI. NUMERICAL RESULTS

We now turn to our numerical study of the temperature dependence of the exciton fluorescence decay time in 1D molecular aggregates, described by the model presented in Sec. II. In all calculations, we have considered an aggregate of 100 molecules, which is a typical exciton coherence

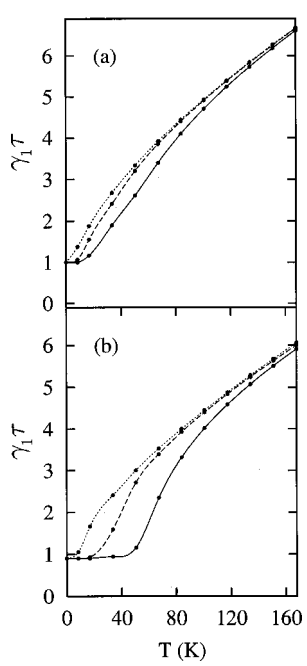

FIG. 1. Temperature dependence of the fluorescence decay time τ measured in units of $1/\gamma_1$ after bottom excitation of an aggregate of length $N=100$ with $J=600\ \mathrm{cm}^{-1}$. The glassy host exciton scattering model was used with scattering strength $W_0^{\mathrm{gl}}/J=10$ (solid), 10^2 (dashed), and 10^4 (dotted). The thicker dots indicate the data points generated in our numerical simulations, while the curves provide a smooth guide to the eye. Data in (a) were calculated using the definition Eq. (22), while in (b), the long-time tail of the total population kinetics was neglected by truncating the integral in Eq. (22) at $t_{\max}$ for which $P(t_{\max})=0.1$.

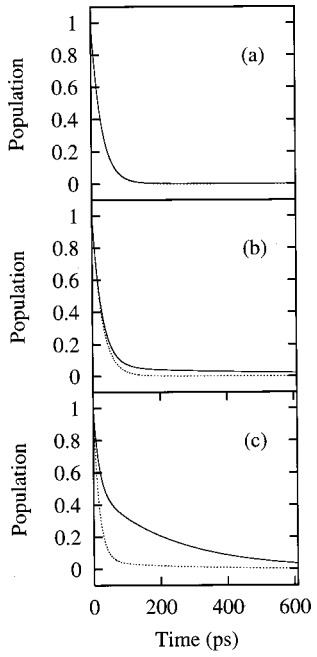

FIG. 2. Kinetics of the total population [$P(t)$, solid line] and the population of the bottom exciton state [$P_1(t)$, dotted line] following bottom excitation of the same aggregate as in Fig. 1 with $W_0^{gl}=10J$ at three different temperatures, $T=17$ K (a), 42 K (b), and 84 K (c). Clearly seen is the occurrence of a long-time tail in $P(t)$ at $T=42$ K, caused by transferring a small amount of the population from the state $k=1$ to the state $k=2$, and its disappearance again at $T=84$ K.

length for cyanine aggregates at low temperature. The monomer radiative rate was set to $\gamma_0=2\times10^{-5}J$, which yields for the radiative rate of the superradiant $k=1$ exciton state $\gamma_1=0.84(N+1)\gamma_0=1.68\times10^{-3}J$. In order to obtain actual time, frequency, and temperature scales, we have used in all our graphs the value $J=600\ \mathrm{cm}^{-1}$ ($1.8\times10^{13}\,\mathrm{s}^{-1}$), which is appropriate for PIC J-aggregates. This translates to $\gamma_0=3.6\times10^{8}\,\mathrm{s}^{-1}$ and $\gamma_1=3.0\times10^{10}\,\mathrm{s}^{-1}$, which are indeed typical of monomer and aggregate radiative decay rates. Finally, it is useful to note that for an aggregate of 100 molecules, the separation between the two lowest exciton states from Eq. (4) is found to be $\Delta\equiv E_2-E_1\approx0.01J$.

We will present results for four types of situations. First, we will consider a glassy host, where we distinguish between initial excitation of the superradiant bottom ($k=1$) state and blue-tail initial excitation. Next, we reconsider both cases for a crystalline host.

A. Glassy host

First of all, let us estimate the value of the parameter W_0^{gl} that distinguishes between the limits of fast and slow relaxation. To this end, we equate $W_{12}(T=0)$ to γ_1. Substituting $E_2-E_1\approx0.01J$ into Eq. (16), one obtains $W_{0\,c}^{\mathrm{gl}}\approx10^5J$. For $W_0^{\mathrm{gl}}>W_{0\,c}^{\mathrm{gl}}$ ($W_0^{\mathrm{gl}}<W_{0\,c}^{\mathrm{gl}}$), we are in the fast (slow) relaxation limit. As argued in the Introduction, we will mostly be interested in the slow limit.

1. Bottom excitation

Figure 1 shows the T dependence of the fluorescence decay time τ for three different values of the exciton scattering strength ($W_0^{\mathrm{gl}}=10J, 10^2J$, and 10^4J), calculated after direct initial excitation of the superradiant state $k=1$. The data presented in Fig. 1(a) were obtained using the definition Eq. (22), where the time-integration was carried out until the total population had decayed to the value $P(t_{\max})=0.005$ (which for all practical purposes agrees with integrating until $t=\infty$), while in Fig. 1(b) we used a relaxed definition, with $P(t_{\max})=0.1$, thus ignoring any long-time tails (cf. Sec. V). For further discussion of this figure, it is convenient to also plot the time dependence of the total population $P(t)$ and the partial populations $P_k(t)$ of the lowest four exciton states ($k=1,\ldots,4$), which is done in Figs. 2 and 3 for three different temperatures, in the case $W_0^{\mathrm{gl}}=10J$.

Analyzing Fig. 1, we first note that all curves yield a $T=0$ decay time that equals the superradiant lifetime, γ_1^{-1}, of state $k=1$ [the small deviation from γ_1^{-1} in Fig. 1(b) is due to the truncation of the integral in Eq. (22)]. This is the natural result, because at zero temperature, the exciton created in the lowest (superradiant) state cannot be scattered to the higher (weakly radiating) states, due to the absence of phonons. Being stuck in the bottom state, the exciton emits a photon on the average after a time γ_1^{-1} has passed, meaning that the fluorescence decay time actually reflects the emission process itself. The fact that at low temperatures, hardly any excitation is transferred to the higher exciton states before emission takes place, is clearly visible in Figs. 2(a) and 3(a).

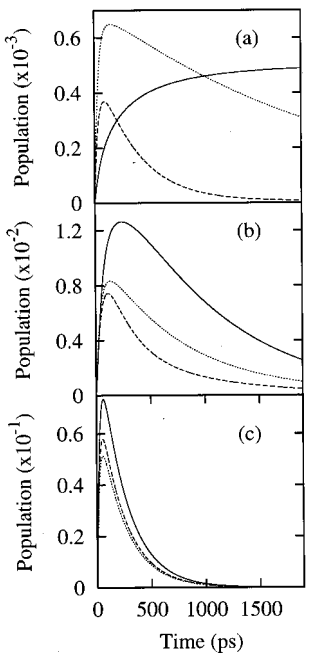

FIG. 3. As Fig. 2, but now are shown the populations of the exciton states $k=2$ (solid), $k=3$ (dashed), and $k=4$ (dotted).

Next, increasing the temperature from $T=0$, we observe a well-pronounced plateau in the value of τ (if $W_0^{\mathrm{gl}} \ll W_{0\,c}^{\mathrm{gl}} = 10^5 J$). The plateau is seen to widen with decreasing W_0^{gl}. The physics of this phenomenon is clear: τ will only increase if the presence of the higher lying dark exciton states becomes noticeable, i.e., if those states actually become populated through exciton–phonon scattering before the energy is spontaneously emitted from the bottom state. Estimating such effects to become visible if 10% of the excitons undergo such scattering before emission, we may calculate the extent, T_{pl}, of the plateau by requiring that $\Sigma_k W_{k1}(T_{\mathrm{pl}}) = 0.1\gamma_1$. The left-hand side in this criterion is the total scattering rate out of the bottom state $k=1$ at $T=T_{\mathrm{pl}}$.

To obtain an analytical estimate of T_{pl}, we first replace the summation over k by an integration according to the standard rule $\Sigma_k \rightarrow [(N+1)/\pi]\int_0^\infty dK$. This step implies that many exciton levels fall within the energy interval $[0,T_{\mathrm{pl}}]$. In view of the nearly quadratic dispersion near the bottom of the exciton band, the values of K that mainly contribute to the integral, are of the order of $K_{\mathrm{pl}}=(T_{\mathrm{pl}}/J)^{1/2}$. As by assumption $K_{\mathrm{pl}} \gg K_1 \equiv \pi/(N+1)$, we thus also typically have $K \gg K_1$, which allows us to approximate $(E_k - E_1)/|J| \approx (3/2 - \ln K)K^2$. Finally, we substitute $\ln K$ by $\ln K_{\mathrm{pl}}$, because this function is changing slowly in the interval close to K_{pl}, where the dominant contribution to the integral comes from. Now, the integral may be performed, to yield

$$\sum_k W_{k,1}(T_{\mathrm{pl}}) = \frac{15 W_0^{\mathrm{gl}}}{16\sqrt{\pi}} \frac{K_{\mathrm{pl}}^7}{(3/2 - \ln K_{\mathrm{pl}})^{1/2}}. \tag{31}$$

Thus, we arrive at a transcendental equation for $K_{\mathrm{pl}} = (T_{\mathrm{pl}}/J)^{1/2}$,

$$\frac{K_{\mathrm{pl}}^7}{(3/2 - \ln K_{\mathrm{pl}})^{1/2}} = \frac{8\sqrt{\pi}}{75} \frac{\gamma_1}{W_0^{\mathrm{gl}}}. \tag{32}$$

If we apply this estimate to $W_0^{\mathrm{gl}} = 10^2 J$ and $W_0^{\mathrm{gl}} = 10J$, we find $T_{\mathrm{pl}} = 28$ K and $T_{\mathrm{pl}} = 52$ K, respectively. These values are in a good agreement with the data presented in Fig. 1(b) and approximately twice as large as those presented in Fig. 1(a). We conclude that the long tail of the total population kinetics, which exists at elevated temperatures due to population of the higher exciton states [cf. Figs. 2(b) and 3(b)] decreases the extent of the plateau by a factor of 2. This is due to the overestimating effect which such tails have on the radiative lifetime defined through Eq. (22) (see discussion in Sec. V).

We note that the estimate Eq. (32) is not applicable to the case $W_0^{\mathrm{gl}} = 10^4 J$, as it yields $T_{\mathrm{pl}} \approx 7.5$ K, which is smaller than the energy difference Δ between the two lowest exciton states. Thus, replacing the k summation by an integration is not allowed for this scattering strength. The small plateau that can still be observed for $W_0^{\mathrm{gl}} = 10^4 J$, originates from the discreteness of the exciton levels.

For temperatures beyond T_{pl}, all curves in Fig. 1 show an increase of τ, due to the population of dark states. As is observed, at higher temperatures all curves approach one asymptotic curve that has an approximate $T^{1/2}$ behavior. The latter reflects two facts: (i) the excitons reach thermal equilibrium before the emission occurs [see Figs. 2(c) and 3(c), where the lowest few exciton states are seen to quickly acquire equal populations] and (ii) the number of states that become populated is approximately proportional to $T^{1/2}$ due to the approximate $(E-E_1)^{-1/2}$ behavior of the density of exciton states near the bottom of the band. A small deviation from the $T^{1/2}$-dependence is expected, because the exact spectrum, Eq. (4), differs logarithmically from the K^2-dependence characteristic for the nearest-neighbor approximation.

We finally note that at higher temperatures and (or) higher scattering strength, the curves in Figs. 1(a) and 1(b) approach each other. This is due to the fact that a large part of the population is then transferred from the initially excited bottom state to the dark states before emission occurs. As a result, there is no special long-time tail in the kinetics of the total population anymore. To illustrate this, consider Figs. 2(b) and 2(c). In the former, a separate long-time tail is still seen to follow the fast initial decay, while in the latter the overall kinetics time scale has become longer.

To complete the discussion for bottom excitation, we briefly consider the alternative definition τ_e for the fluorescence decay time. The corresponding results are plotted in Fig. 4. As in Fig. 1, we observe a plateau, whose extent correlates well with that in Fig. 1(b). This confirms our observation below Eq. (29) that the measure τ_e does not suffer from the slow-tail problem. However, beyond the plateau, the curves in Fig. 4 differ drastically from those in Fig. 1 and are counterintuitive, as they go down instead of up. This is due to a rapid decrease of the emission intensity, not because of radiation from the bottom state, but because population is rapidly transferred from this state to the higher lying dark states [see discussion below Eq. (30)]. This is illustrated clearly by Fig. 5, which shows $I(t)$ for four temperatures at

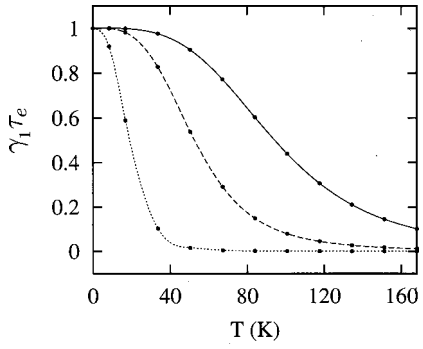

FIG. 4. Temperature dependence of the fluorescence decay time τ_e defined in Eq. (21), calculated for the same system and conditions as in Fig. 1. Curves labeled as in Fig. 1.

$W_0^{\mathrm{gl}}=10^4J$. With increasing temperature, the initial decay of the intensity becomes faster, while its tail (reached after equilibration) slows down. The latter is the intuitive effect on the radiative decay time, but this is not captured by the decay time τ_e.

2. Blue-tail excitation

We now turn to the case where the initial excitation takes place above the bottom of the exciton band. Then spontaneous emission can only occur after the exciton has relaxed to the bottom state. Obviously, in the slow-relaxation limit this may cause a bottleneck for the emission process. This reflects itself in a particular temperature dependence of the fluorescence decay time. In Fig. 6 we depict $\tau(T)$, calculated using Eq. (22), for initial excitation of the $k_i=7$ exciton state for $W_0^{\mathrm{gl}}=10^4J$. Clearly, the observed behavior differs drastically from the one found for bottom state excitation, in particular at low temperatures. First of all, at $T=0$, τ deviates from γ_1^{-1}, which for bottom excitation was always found to be the zero-temperature decay rate. Furthermore, the curve shows a region where τ decreases upon increasing T. The noted peculiarities originate from the interplay between intraband relaxation and spontaneous emission. We will clarify this further by estimating the scattering rates W_{k7} that feature in this interplay for $T=0$.

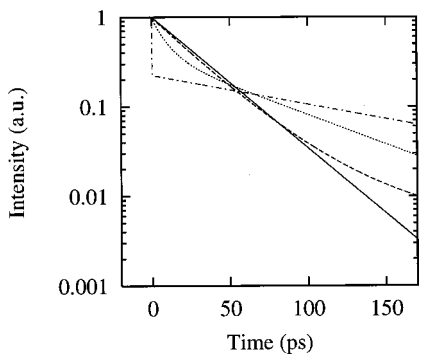

FIG. 5. Fluorescence intensity as a function of time for the same system as in Fig. 1, using bottom excitation and a scattering strength $W_0^{\mathrm{gl}}=10^4J$. Curves correspond to $T=0$ K (solid), 8 K (dashed), 17 K (dotted), and 84 K (dashed–dotted).

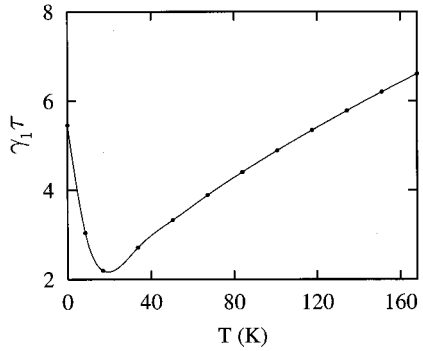

FIG. 6. Temperature dependence of the fluorescence decay time τ [Eq. (22)] for an aggregate of length $N=100$ with $J=600\ \mathrm{cm}^{-1}$ after initial excitation of the $k=7$ state. The glassy-host exciton scattering model was used with scattering strength $W_0^{\mathrm{gl}}=10^4J$. The dots indicate the data points generated in our numerical simulations, while the curve provides a smooth guide to the eye.

Due to the cubic dependence of W_{kk_i} on $|E_k-E_{k_i}|$ [Eq. (16)], the transitions from the initial exciton state k_i to the ones with quantum numbers $k=1$ and 2 are the most probable; moreover, the corresponding rates are almost equal to each other. This is because E_7-E_1 and E_7-E_2 both are of the order of $0.1J$, while they differ from each other by $\Delta\approx 0.01J$. For estimates, we will use $E_7=-2.3J$, which for $N=100$ leads to the $W_{17}\approx W_{27}\approx 10^{-5}W_0^{\mathrm{gl}}$. Thus, for our example case of $W_0^{\mathrm{gl}}=10^4J$, we arrive at $W_{17}\approx 0.1J\approx 10^2\gamma_1$. This means that the population from the initially excited state is transferred rapidly (on the scale of γ_1^{-1}) to the states $k=1$ and $k=2$. The $k=1$ state decays radiatively with the rate γ_1, while the $k=2$ state only decays via relaxation to the $k=1$ state. The rate of the latter process is given by $W_{12}\approx 0.1\gamma_1$. This relationship between the dominant rates leads to a biexponential kinetics of the total population; a fast decay with a time constant $\sim\gamma_1^{-1}$, followed by a slow decay with time constant $\sim W_{12}^{-1}$. This analysis is nicely confirmed by Fig. 7, in which the kinetics of the total population $P(t)$ as well as the partial populations $P_1(t)$ and $P_2(t)$ states are shown. Both exponentials are seen to have comparable weight, as was to be expected, because the relaxation rates from the excited state $k_i=7$ into the states $k=1$ and $k=2$ are

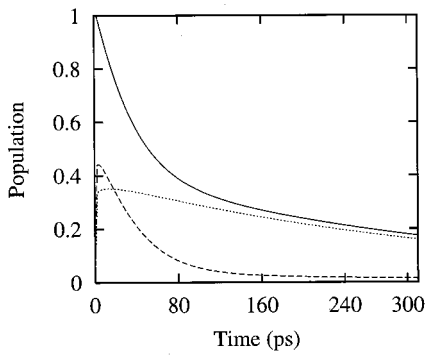

FIG. 7. Zero-temperature kinetics of the total population $P(t)$ (solid line) and the populations $P_1(t)$ (dashed) and $P_2(t)$ (dotted) of the two lowest exciton states for the same system and conditions as considered in Fig. 6. The figure clearly shows a biexponential behavior of $P(t)$.

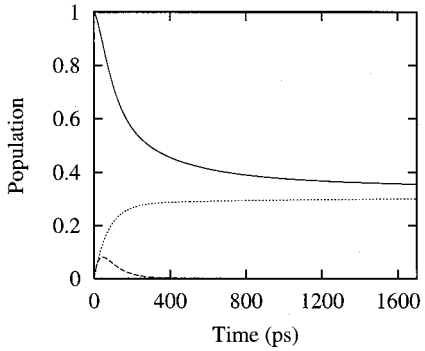

FIG. 8. As Fig. 7, but now for $W_0^{\mathrm{gl}}=10J$.

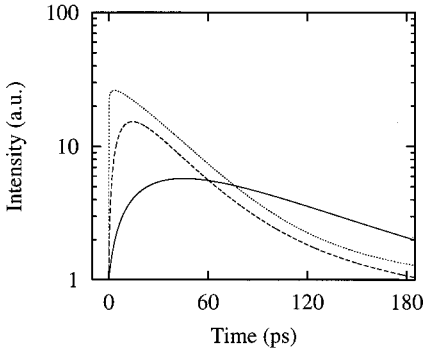

FIG. 10. Fluorescence intensity as a function of time for an aggregate of length $N=100$ with $J=600\ \mathrm{cm}^{-1}$ after initial excitation of the $k=7$ state. The glassy-host exciton scattering model was used with scattering strength $W_0^{\mathrm{gl}}/J=10$ (solid), 10^2 (dashed), and 10^4 (dotted).

roughly equal. As a consequence, the integrated contribution of the slow component dominates over the one deriving from the fast component, which explains why the value of $\tau(T=0)$ in Fig. 6 is larger than γ_1^{-1}. The same arguments explain why at low temperature τ goes down upon increasing T; this is simply due to the fact that W_{12} increases with increasing the temperature, so that the contribution of the slower component to τ diminishes. If temperature increases further, W_{12} becomes larger than γ_1 and we approach the limit of fast (on the time scale of emission) equilibration. Then $\tau(T)$ should not strongly depend on the initial condition anymore, which is why Fig. 6 at higher temperatures is very similar to Fig. 1.

At small W_0^{gl}, the decay scenario differs from the one described above. Let us, for instance, take $W_0^{\mathrm{gl}}=10J$, so that $W_{17}\approx 10^{-4}J\approx 0.1\gamma_1$. Now, the intraband relaxation is so slow that it completely governs the total population decay. Again, a biexponential behavior is found in the population kinetics, with the fast component now being limited by the rate W_{17}, while the slow one is again characterized by the (now very slow) rate W_{12}. This limit of extremely slow relaxation is illustrated in Fig. 8.

Finally, we address the T-dependence of the decay time defined by τ_e [Eq. (21)]. The results are presented in Fig. 9 for three scattering strengths and, for further clarification, the corresponding kinetics at $T=0$ is shown in Fig. 10. At short times, before the excitation is scattered to the band bottom, the intensity is very small, as the emission rate γ_7 is small [Eq. (5)]. The intensity then grows due to population of the bottom state(s) through intraband relaxation and, after reaching a maximum, it finally decays again with a rate that may be interpreted as the relaxed exciton's radiative rate. This results in a temperature dependence of τ_e that is again characterized by a low-temperature plateau. This plateau only occurs at $\tau_e=\gamma_1^{-1}$ if the relaxation is sufficiently fast to bring all population down to the bottom state before emission from it starts. For the small scattering strength $W_0^{\mathrm{gl}}=10J$, this is seen not to be the case. In contrast to the case of bottom excitation (Fig. 4), the plateau is generally followed by an increasing decay time. The reason is that now the populations of all exciton levels have indeed equilibrated by the time the spontaneous decay from the bottom state starts. This is not the case for $W_0^{\mathrm{gl}}=10J$, which explains the more complicated T dependence observed in Fig. 9.

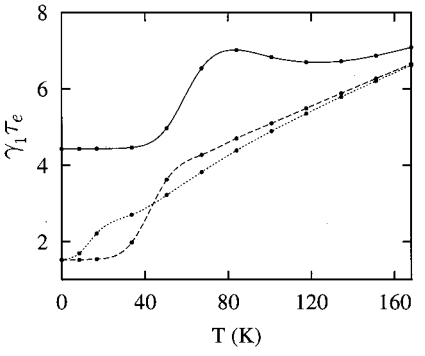

FIG. 9. As Fig. 6, except that now τ_e [Eq. (21)] has been used as measure of the fluorescence decay time. Curves correspond to the scattering strength $W_0^{\mathrm{gl}}/J=10$ (solid), 10^2 (dashed), and 10^4 (dotted).

B. Crystalline host

Similar to the case of the glassy-host model of exciton–phonon scattering, we have carried out a series of numerical calculations for the crystalline-host model. In many respects, the essential physics within both models is the same and we will therefore discuss in detail only the new features, dealing with the already discussed phenomena only in passing.

As before, we first estimate the value of W_0^{cr} that distinguishes between the limits of fast and slow relaxation. Recall that this implies equating $W_{12}(T=0)$ to γ_1. Using in Eq. (19) with $k=1$, $k'=2$ the approximations $\sin[\pi/(N+1)]\approx\pi/(N+1)$, $\sin[2\pi/(N+1)]\approx 2\pi/(N+1)$, $E_2-E_1\approx 0.01|J|$, and $f(X)=1$, we arrive at $W_{0\,c}^{\mathrm{cr}}\approx 10^5 J$, which happens to be equal to the critical scattering strength for the glassy-host model.

1. Bottom excitation

In Fig. 11 we depict $\tau(T)$, calculated after direct initial excitation of the bottom exciton state, for three different scattering strengths: $W_0^{\mathrm{cr}}=10^2J$, 10^3J, and 10^4J. Figure 11(a) shows the results using the definition Eq. (22) by integrating up to the time $t_{\max}$, where the total exciton population has decayed to $P(t_{\max})=0.005$ (i.e., up to $t=\infty$ for all practical purposes), while in Fig. 11(b) the slow-tail contribution to τ

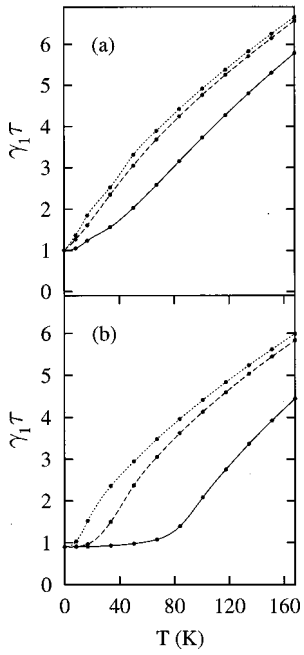

FIG. 11. As Fig. 1, but now using the crystalline-host model for exciton scattering. Curves correspond to scattering strengths $W_0^{cr}/J=10^2$ (solid), 10^3 (dashed), and 10^4 (dotted).

is discarded by integrating only until the time at which $P(t_{max})=0.1$. As in the case of the glassy host (Fig. 1), all curves start from the same point (corresponding to the radiative lifetime γ_1^{-1} of the superradiant state $k=1$), then show a plateau, and finally go up with increasing temperature.

As in Sec. VI A 1, we estimate the extent T_{pl} of the plateau by equating $\Sigma_k W_{k1}(T_{pl})$ to $0.1\gamma_1$. Substituting $(E_k-E_1)/(\cos K-\cos K_1)\approx 2J(3/2-\ln K)$ [typically $K\gg K_1\equiv\pi/(N+1)$] and performing the summation over k in a manner similar to the glassy-host model, one obtains

$$K_{pl}^5(3/2-\ln K_{pl})^{5/2}=\frac{(N+1)^3}{60\pi^{3/2}}\frac{\gamma_1}{W_0^{cr}}, \tag{33}$$

where $K_{pl}=(T_{pl}/J)^{1/2}$. Solving this equation for $W_0^{cr}=10^2J, 10^3J$, and 10^4J, we find as estimates $T_{pl}=100$ K, 34 K, and 11 K, respectively, in good agreement with the numerical data in Fig. 11(b). We note that T_{pl} is larger than obtained within the glassy-host model at the same scattering strength W_0. This results from the fact that within the crystalline-host model, $W_{kk'}$ increases more slowly with $|E_k-E_{k'}|$ than within the glassy-host model.

2. Blue-tail excitation

Without showing figures, we mention that the temperature dependence of τ for blue-side excitation exhibits the same general behavior as in the case of a glassy host. In particular, we again find that (i) the zero-temperature value of τ [calculated through Eq. (22)] deviates from γ_1^{-1} and (ii) a region exists where τ decreases with increasing T. As in Sec. VI A 2, the physical interpretation of these peculiarities is based on the interplay of intraband relaxation and emission processes. However, the scenario of the intraband relaxation in the present model differs considerably from that in the glassy-host model. While in the latter we found that relaxation from the excitation window directly to the bottom of the band has the highest probability, in the present case, the relaxation occurs preferably through several intermediate states, which may, in fact, act as a bottleneck. We will show this below.

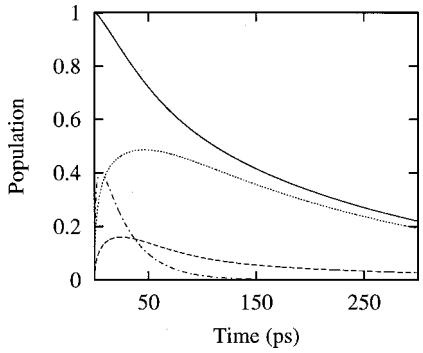

FIG. 12. Zero-temperature kinetics of the total population $P(t)$ (solid line) and the populations $P_1(t)$ (dashed), $P_2(t)$ (dotted), and $P_3(t)$ (dashed–dotted) of the three lowest exciton states for an aggregate of $N=100$ molecules with $J=600$ cm^{-1} after initial excitation of the $k=7$ state. The crystalline-host exciton scattering model was used with scattering strength $W_0^{cr}=10^4J$.

Let us analyze the zero-temperature relaxation rate from an initially excited exciton state k_i to a low-lying state k. For the sake of simplicity, we will use several approximations: (i) the nearest-neighbor approximation for the exciton energy spectrum, $E_k=-2J+JK^2$, (ii) $f(X)=1$, and (iii) $k_i, k\ll N$. Then, the scattering rate Eq. (19) takes the form,

$$W_{kk_i}=\frac{16W_0^{cr}K_1^6}{(N+1)^2}k_i^2k^2(k_i^2-k^2), \tag{34}$$

which reaches its maximum at $k^2=k_i^2/2$: $W_{k_i/\sqrt{2},k_i}=[W_0/4(N+1)^2]K_1^6k_i^6$. This scattering rate is to be compared with the one to the superradiant state with $k=1$. Neglecting 1 as compared to k_i^2 in the last factor of Eq. (34) for $k=1$, one obtains

$$W_{1k_i}=\frac{16W_0^{cr}K_1^6}{(N+1)^2}k_i^4=\frac{4}{k_i^2}W_{k_i/\sqrt{2},k_i}, \tag{35}$$

i.e., $W_{1k_i}\ll W_{k_i/\sqrt{2},k_i}$. From this we conclude that jumping directly to the bottom state is unlikely, so that after excitation in a high-lying state, the exciton has to make several relaxation steps to reach the superradiant $k=1$ state. In the limit of fast relaxation, $W_{12}>\gamma_1$, this will certainly occur and it will do so before the exciton decays through spontaneous emission. By contrast, in the slow-relaxation limit, $W_{12}<\gamma_1$, the stepwise relaxation may be stopped at some intermediate band state k' and the exciton may never reach the bottom state. The reason is that each step downhill decreases the relaxation rate by a factor of 8 [cf. Eq. (34)], so that at some point the rate for making the next step, $\Sigma_k W_{kk'}$, may become comparable to or smaller than the spontaneous emission rate from the corresponding state, $\gamma_{k'}$. Then, $\gamma_{k'}$ will determine the exciton fluorescence decay time.

Figure 12 nicely illustrates the above described scenario

of relaxation. Here, we plotted the numerically calculated zero-temperature kinetics of the total population $P(t)$ as well as the partial populations $P_k(t)$ for $k=1$, 2, and 3 using a scattering strength $W_0^{\rm cr}=10^4J$ and $k_i=7$ for the initially excited exciton state. Indeed it is seen that at the early stage of the kinetics only a small part of the initial population is transferred to the bottom state $k=1$, while the higher states $k=2$ and 3 accumulate almost all population. After this early population transfer, the $k=3$ state first relaxes to the states $k=2$ and $k=1$. This becomes clear from the values of W_{13} and W_{23}, which from Eq. (19) with the present parameters ($W_0^{\rm cr}=10^4J$ and $N=100$) are found to be $W_{13}=1.24\times10^{-3}J$ and $W_{23}=0.62\times10^{-3}J$. At the same time, the radiative decay rate of the $k=3$ state equals $\gamma_3=\gamma_1/9=0.19\times10^{-3}J$, which is an order of magnitude smaller than the total radiationless relaxation rate of this state, $W_{13}+W_{23}\approx1.86\times10^{-3}J$ (0.034 ps^{-1} in frequency units). Thus, the rate $W_{13}+W_{23}$ is expected to govern the decay of the $k=3$ state, which is in perfect agreement with the numerical data in Fig. 12. Finally, the $k=2$ state slowly relaxes to the $k=1$ state ($W_{12}^{-1}\approx10\gamma_1^{-1}\approx300$ ps), determining the long-tail decay of the total population. Also this time scale shows excellent agreement with the numerical data.

VII. SUMMARY AND CONCLUDING REMARKS

In this paper, we numerically studied the temperature dependence of the fluorescence decay time of 1D Frenkel excitons in J-aggregates resulting from their vibration-assisted redistribution over the exciton band after pulsed excitation of a subset of states. The redistribution was modeled using a Pauli master equation that accounts for the scattering between exciton levels. We considered two models for the scattering rates in this equation. In one we assumed the host medium to have a glassy (disordered) character, while in the other it was assumed to be crystalline. It appeared that the exciton scattering rates, corresponding to these two models, differ considerably from each other.

We have paid particular attention to the definition of the *fluorescence* decay time and its relation to the *radiative* decay time. We have considered two definitions. The first (τ) is the expectation time of photon emission, which equals the time-integrated kinetics of the total exciton population $P(t)$, while the second (τ_e) uses the $1/e$ time of the fluorescence intensity $I(t)=-\dot{P}(t)$, as is often done in experiments. We have shown that for an exciton system in the presence of intraband relaxation, it is sometimes difficult to extract information on the radiative decay time on the basis of measurements of the fluorescence kinetics. The potential pitfalls that may mask the real radiative decay time have been elucidated using a simple model that contains only two exciton states as well as by analyzing numerical results for linear J-aggregates for various initial conditions and exciton–phonon scattering strengths.

We have found that, independently of the intraband scattering model, the interplay between the intraband relaxation and the superradiant decay in combination with the type of fluorescence excitation (direct excitation of the superradiant bottom state or initial excitation of higher-lying weakly radiating states), crucially affects the physics of the fluorescence kinetics. For bottom excitation and at zero temperature, the exciton remains in the superradiant state until the radiative relaxation occurs. Upon increasing the temperature, population is transferred to the higher-energy weakly radiating states, giving rise to a slowing down of the radiative decay. This process only starts when the vibration-assisted scattering rate from the bottom exciton state to the higher ones approaches the superradiant emission rate. As a result, the temperature dependence of the fluorescence decay time shows a plateau that extends further for slower intraband scattering strength. In the plateau region, the superradiant damping rate determines the fluorescence decay. Beyond the plateau, the fluorescence decay time goes up with increasing temperature and eventually approaches a $T^{1/2}$-scaling. The latter reflects the fact that the excitons arrive at thermal equilibrium within the time scale of photon emission. Under these conditions, the fluorescence lifetime τ reflects the exciton *radiative lifetime*, while the decay time τ_e at higher temperatures measures the upward scattering rate from the bottom state, rather than the radiative decay time.

In the case of initial excitation of high-lying exciton states, the physical picture of the exciton emission process strongly depends on the ratio of the rates for intraband scattering and exciton superradiance. If the former is faster than the latter, the excitons created initially in the weakly radiating states are rapidly (on the scale of the exciton superradiant emission) transferred to the superradiant state. The subsequent dynamics of emission is similar to the one found for direct excitation of the bottom state. By contrast, if the intraband scattering is slower than the superradiant emission, the former represents the bottleneck for radiative decay and determines the exciton fluorescence decay time. In particular, the zero-temperature value of the fluorescence decay time may then considerably deviate from the superradiant value. Furthermore, under these conditions, the fluorescence decay time may actually go down with increasing temperature at small temperatures, because the fluorescence kinetics at low temperatures then simply reflects the slow intraband relaxation, rather than the exciton radiative rate. At higher temperatures the fluorescence decay time eventually approaches again the $T^{1/2}$-behavior, because the vibration-assisted relaxation rates increase and the excitons arrive at thermal equilibrium before emission.

The above conclusions lead to the general important observation that was anticipated in the Introduction already, namely that time-resolved fluorescence experiments do not necessarily measure the exciton radiative lifetime. Whether or not they do, apparently depends on the excitation condition and the rate of intraband relaxation as compared to the rate of exciton radiative emission. In particular, for excitation high in the exciton band under conditions of slow relaxation [which seems to be relevant to PIC (Ref. 23)], the fluorescence experiment measures the intraband relaxation rate. This conclusion is of special importance at low temperatures, when the exciton subsystem after excitation is far from thermal equilibrium. This also has obvious implications for the possibility to extract the low-temperature exciton coherence length from radiative lifetime measurements. If the intraband

relaxation is slow, this cannot be done using blue-tail excitation. Rather, only resonant excitation of the fluorescence will then give the desired information, as this directly probes the optically active states characterized by the exciton coherence length. Alternatively, resonant pump–probe spectroscopy may be used to obtain this information.[30–32]

ACKNOWLEDGMENTS

One of the authors (M.B.) gratefully acknowledges Nuffic for financial support through a Huygens Fellowship. V.A.M. acknowledges support from the University of Groningen and from the Spanish Ministerio de Educación, Cultura y Deporte (Project No. SAB2000-0103). This work was partially supported by INTAS (project 97-10434).

APPENDIX A: DERIVATION OF THE EXCITON-VIBRATION COUPLING

We start with the Hamiltonian in the form,[2]

$$H_{\mathrm{ex-vib}}=\sum_{n=1}^{N}\sum_{s}\ \delta U_{sn}|n\rangle\langle n|, \tag{A1a}$$

$$\delta U_{sn}=\left(\frac{\partial U_{sn}}{\partial \mathbf{R}_{sn}}\right)_0\cdot(\delta\mathbf{R}_s-\delta\mathbf{R}_n). \tag{A1b}$$

Here, U_{sn} is the interaction of the excited aggregate molecule n with a surrounding molecule s (either a host molecule or another aggregate molecule, the latter being in its ground state). Furthermore, δU_{sn} is the variation of this energy resulting from the displacements, $\delta\mathbf{R}_s$ and $\delta\mathbf{R}_n$, of these molecules from their equilibrium positions. The subscript ''0'' denotes that the derivative must be taken at the equilibrium value of $\mathbf{R}_{sn}$.

We express the displacement operators in terms of operators of the normal vibration modes, labeled q, in the standard way ($\hbar=1$)

$$\delta\mathbf{R}_n=\sum_q\left(\frac{1}{2\omega_q}\right)^{1/2}\mathbf{Q}_{nq}a_q+\mathrm{h.c.} \tag{A2}$$

Here, ω_q and $\mathbf{Q}_{nq}$ are, respectively, the eigenfrequencies and eigenvectors of the vibration Hamiltonian of the entire system (host+aggregates), and a_q ($a_q^\dagger$) is the annihilation (creation) operator of this mode. Within the normal mode representation, the Hamiltonian (A1a) takes the form,

$$H_{\mathrm{ex-vib}}=\sum_{n=1}^{N}\sum_{q}\ V_{nq}|n\rangle\langle n|a_q+\mathrm{h.c.}, \tag{A3a}$$

$$V_{nq}=\sum_s\left(\frac{1}{2\omega_q}\right)^{1/2}\left(\frac{\partial U_{sn}}{\partial\mathbf{R}_{sn}}\right)_0\cdot(\mathbf{Q}_{sq}-\mathbf{Q}_{nq}). \tag{A3b}$$

As motivated in the main text, we focus on the coupling of excitons to acoustic phonons, in which case the $\mathbf{Q}_{nq}$ are represented by plane waves,

$$\mathbf{Q}_{nq}=\left(\frac{1}{M}\right)^{1/2}\mathbf{u}_q e^{i\mathbf{q}\cdot\mathbf{R}_n}, \tag{A4}$$

where the mode index $q=(\mathbf{q},\alpha)$ specifies the wave number ($\mathbf{q}$) and polarization ($\alpha=1,2,3$) of the acoustic phonons, M is the mass of the total system, and $\mathbf{u}_q$ is the polarization vector of the acoustic mode q. Note that, in contrast to the case of optical phonons, $\mathbf{u}_q$ does not depend on the molecular position. The dispersion relation in the long-wavelength limit is given by $\omega_q=v_\alpha|\mathbf{q}|$, $v_1=v_2=v_t$ and $v_3=v_l$ being the speed of transverse and longitudinal sound, respectively.

Substituting Eq. (A4) into Eq. (A3b), we obtain

$$V_{nq}=\left(\frac{1}{2M\omega_q}\right)^{1/2}e^{i\mathbf{q}\cdot\mathbf{R}_n}\sum_s\left(\frac{\partial U_{sn}}{\partial\mathbf{R}_{sn}}\mathbf{u}_q\right)_0\times[e^{i\mathbf{q}\cdot(\mathbf{R}_s-\mathbf{R}_n)}-1]. \tag{A5}$$

As U_{sn} decreases fast with increasing distance $|\mathbf{R}_{sn}|$, only the nearest surroundings contribute to the sum in Eq. (A5). As a result, we may expand the exponential inside this sum, keeping only the first two terms. Doing so and using the dispersion relation $\omega_q=v_\alpha|\mathbf{q}|$, we get

$$V_{nq}=i\left(\frac{|\mathbf{q}|}{2Mv_\alpha}\right)^{1/2}\chi_{nq}\,e^{i\mathbf{q}\cdot\mathbf{R}_n}, \tag{A6}$$

where we introduced

$$\chi_{nq}=\sum_s\left(\frac{\partial U_{sn}}{\partial\mathbf{R}_{sn}}\mathbf{u}_q\right)_0\frac{\mathbf{q}\cdot(\mathbf{R}_s-\mathbf{R}_n)}{|\mathbf{q}|}. \tag{A7}$$

In a crystalline host medium, χ_{nq} does not depend on the position of the molecule in the aggregate, while it is a stochastic function of this position in the case of a disordered host medium. It should be noted that χ_{nq} depends only on the orientation of the phonon wave vector $\mathbf{q}$. Moreover, due to the summation over many surrounding molecules, this dependence is expected to be rather smooth.

APPENDIX B: NUMERICAL ALGORITHM FOR SOLVING THE PAULI MASTER EQUATION

To solve the Pauli master equation Eq. (11), we use the numerical procedure proposed in Ref. 24, based on passing from the equation's differential form to its integral version,

$$P_k(t)=P_k(0)e^{-W_kt}+\sum_{k'}\ W_{kk'}\int_0^t dt'\,e^{-W_k(t-t')}P_{k'}(t'). \tag{B1}$$

Here, $W_k=\gamma_k+\Sigma_{k'}W_{k'k}$ is the total rate of population loss from state k, both due to scattering and due to spontaneous emission. The equivalence of Eq. (B1) to Eq. (11) is proved by straightforward differentiation of the former. Next, using Eq. (B1), one relates $P_k(t+dt)$ to $P_k(t)$ through

$$P_k(t+\delta t)=P_k(t)e^{-W_k\delta t}+\frac{1}{W_k}(1-e^{-W_k\delta t})\times\sum_{k'}\ W_{kk'}P_{k'}(t). \tag{B2}$$

Finally, to avoid divergencies at small W_k in Eq. (B2), we expand

$$\frac{1}{W_k}(1-e^{-W_k\delta t})=\delta t\left(1-\frac{1}{2}\,W_k\delta t\right). \tag{B3}$$

The iteration procedure defined by Eq. (B2) in combination with Eq. (B3) turned out to provide a stable numerical algorithm to solve the master equation.

[1] J. Frenkel, Phys. Rev. **17**, 17 (1931).
[2] A. S. Davydov, *Theory of Molecular Excitons* (Plenum, New York, 1971).
[3] F. C. Spano and J. Knoester, in *Advances in Magnetic and Optical Resonance*, edited by W. S. Warren (Academic, New York, 1994), Vol. 18, p. 117.
[4] Contributions in Adv. Mater. **7**, 435–512 (1995).
[5] *J-aggregates*, edited by T. Kobayashi (World Scientific, Singapore, 1996).
[6] F. C. Spano and S. Mukamel, J. Chem. Phys. **91**, 683 (1989).
[7] H. Fidder, J. Knoester, and D. A. Wiersma, J. Chem. Phys. **95**, 7880 (1991).
[8] V. A. Malyshev, Opt. Spektr. **71**, 873 (1991) [Opt. Spectrosc. **71**, 505 (1991)]; J. Lumin. **55**, 225 (1993).
[9] A. I. Zaitsev, V. A. Malyshev, and E. D. Trifonov, Zh. Exp. Teor. Fiz. **84**, 475 (1983) [Sov. Phys. JETP **57**, 275 (1983)].
[10] V. M. Agranovich and O. A. Dubovskii, ZhETF Pis'ma **3**, 345 (1966) [JETP Lett. **3**, 223 (1966)].
[11] S. de Boer and D. A. Wiersma, Chem. Phys. Lett. **165**, 45 (1990).
[12] H. Fidder, J. Knoester, and D. A. Wiersma, Chem. Phys. Lett. **171**, 529 (1990).
[13] H. Fidder, J. Terpstra, and D. A. Wiersma, J. Chem. Phys. **94**, 6895 (1991).
[14] H. Fidder, ''Collective optical response of molecular aggregates,'' Ph.D. thesis, University of Groningen, Groningen, 1993.
[15] H. Fidder and D. A. Wiersma, Phys. Status Solidi B **188**, 285 (1995).
[16] J. Moll, S. Daehne, J. R. Durrant, and D. A. Wiersma, J. Chem. Phys. **102**, 6362 (1995).
[17] V. F. Kamalov, I. A. Struganova, and K. Yoshihara, J. Phys. Chem. **100**, 8640 (1996).
[18] I. G. Scheblykin, M. M. Bataiev, M. Van der Auweraer, and A. G. Vitukhnovsky, Chem. Phys. Lett. **316**, 37 (2000).
[19] F. C. Spano, J. R. Kuklinsky, and S. Mukamel, Phys. Rev. Lett. **65**, 211 (1990); J. Chem. Phys. **94**, 7534 (1991).
[20] E. O. Potma and D. A. Wiersma, J. Chem. Phys. **108**, 4894 (1998).
[21] J. Feldmann, G. Peter, E. O. Göbel, P. Dawson, K. Moore, C. Foxon, and R. J. Elliott, Phys. Rev. Lett. **59**, 2337 (1987).
[22] H. von Berlepsch, C. Böttcher, and L. Dähne, J. Phys. Chem. B **104**, 8792 (2000).
[23] M. Bednarz, V. A. Malyshev, J. P. Lemaistre, and J. Knoester, J. Lumin. **94/95**, 271 (2001).
[24] A. J. van Strien, J. Schmidt, and R. Silbey, Mol. Phys. **46**, 151 (1982).
[25] H. Benk and R. Silbey, J. Chem. Phys. **79**, 3487 (1983).
[26] J. A. Leegwater, J. R. Durrant, and D. R. Klug, J. Phys. Chem. B **101**, 7205 (1997).
[27] O. Kühn and V. Sundström, J. Phys. Chem. B **101**, 3432 (1997); J. Chem. Phys. **107**, 4154 (1997).
[28] V. Malyshev and P. Moreno, Phys. Rev. B **51**, 14587 (1995).
[29] J. P. Lemaistre, J. Lumin. **76&77**, 437 (1998); Chem. Phys. **246**, 283 (1999).
[30] G. Juzeliūnas, Z. Phys. D: At., Mol. Clusters **8**, 379 (1988).
[31] T. Meier, V. Chernyak, and S. Mukamel, J. Phys. Chem. B **101**, 7332 (1997).
[32] L. D. Bakalis and J. Knoester, J. Phys. Chem. B **103**, 6620 (1999).